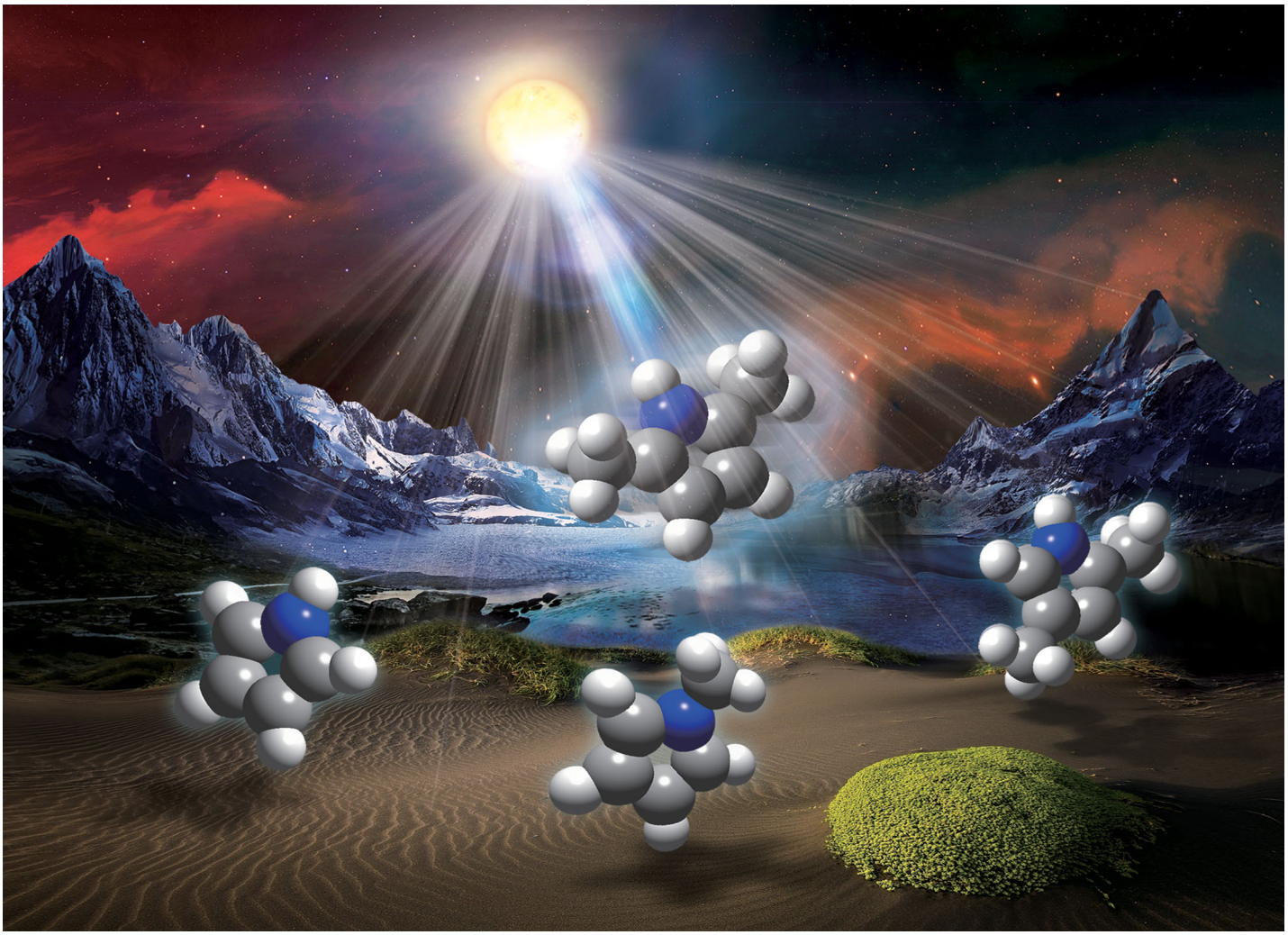

Showcasing research from the Group of Prof. Guorong Wu at Dalian Institute of Chemical Physics, Chinese Academy of Sciences, China

Ultrafast excited-state dynamics of 2,5-dimethylpyrrole

This paper reports a detailed investigation on the ultrafast excited-state dynamics of 2,5-dimethylpyrrole following deep UV excitation, studied using a femtosecond time-resolved photoelectron imaging method. The methyl substitution effects on the decay dynamics of the excited states of pyrrole are discussed, adding new insights into the photochemistry of a range of important heteroaromatic molecules.

As featured in:

See Guorong Wu *et al.*, *Phys. Chem. Chem. Phys.*, 2018, **20**, 15015.

ROYAL SOCIETY OF CHEMISTRY

rsc.li/pccp

Registered charity number: 207890

PCCP

PAPER

View Article Online
View Journal | View Issue

Cite this: *Phys. Chem. Chem. Phys.*, 2018, **20**, 15015

Ultrafast excited-state dynamics of 2,5-dimethylpyrrole

Dongyuan Yang,[ab] Yanjun Min,[ab] Zhichao Chen,[a] Zhigang He,[a] Kaijun Yuan,[a] Dongxu Dai,[a] Xueming Yang[a] and Guorong Wu*[a]

Received 7th February 2018,
Accepted 29th March 2018

DOI: 10.1039/c8cp00883c

rsc.li/pccp

The ultrafast excited-state dynamics of 2,5-dimethylpyrrole following excitation at wavelengths in the range of 265.7–216.7 nm is studied using the time-resolved photoelectron imaging method. It is found that excitation at longer wavelengths (265.7–250.2 nm) results in the population of the $S_1(^1\pi\sigma^*)$ state, which decays out of the photoionization window in about 90 fs. At shorter pump wavelengths (242.1–216.7 nm), the assignments are less clear-cut. We tentatively assign the initially photoexcited state(s) to the $^1\pi3p$ Rydberg state(s) which has lifetimes of 159 ± 20, 125 ± 15, 102 ± 10 and 88 ± 10 fs for the pump wavelengths of 242.1, 238.1, 232.6 and 216.7 nm, respectively. Internal conversion to the $S_1(^1\pi\sigma^*)$ state represents at most a minor decay channel. The methyl substitution effects on the decay dynamics of the excited states of pyrrole are also discussed. Methyl substitution on the pyrrole ring seems to enhance the direct internal conversion from the $^1\pi3p$ Rydberg state to the ground state, while methyl substitution on the N atom has less influence and the internal conversion to the $S_1(\pi\sigma^*)$ state represents a main channel.

I Introduction

Pyrrole is a typical model molecule for the understanding of the electronic structure and photochemistry of a range of important biomolecules, such as porphyrins, aromatic amino acids and DNA bases.[1–8] In the last few years, we have investigated the ultrafast excited-state dynamics of pyrrole[9] and two of its methyl-substituted derivatives, *N*-methylpyrrole (NMP)[10] and 2,4-dimethylpyrrole (2,4-DMP),[11] following excitations in the near ultraviolet (UV) region of their respective electronic absorption spectra. Most of the results derived from those studies can be rationalized within the framework proposed by Domcke and coworkers[3,4] and the role of the lowest-lying $S_1(^1\pi\sigma^*)$ state in the non-radiative decay of the excited states was confirmed. In this paper, we report our continuing efforts on this topic and present the investigation of the ultrafast excited-state dynamics of another pyrrole methylated derivative, 2,5-dimethylpyrrole (2,5-DMP). The motivations are similar to those for the previous studies. Besides studying the ultrafast excited-state dynamics of pyrrole's methylated derivatives with increasing complexity, we try to understand the methyl substitution effects on the ultrafast excited-state dynamics of pyrrole, which may aid the development of simple models of such dynamics extendable to larger molecules.

The UV absorption spectrum of 2,5-DMP has been reported before, but no detailed analysis has been provided.[12] As shown in Fig. 1, the main features of this spectrum are similar to those of pyrrole. But the sharp peaks corresponding to the transitions to Rydberg states, especially the $B_1(^1\pi3p_y)$ state, are absent, and this was found to be due to reduced oscillator strengths in a previous calculation.[13] An analogous analysis to that of pyrrole can be made. As suggested by a reinterpretation of the electronic spectrum of pyrrole by Neville and Worth,[14] the broad, strong absorption band between 210–250 nm should be dominated

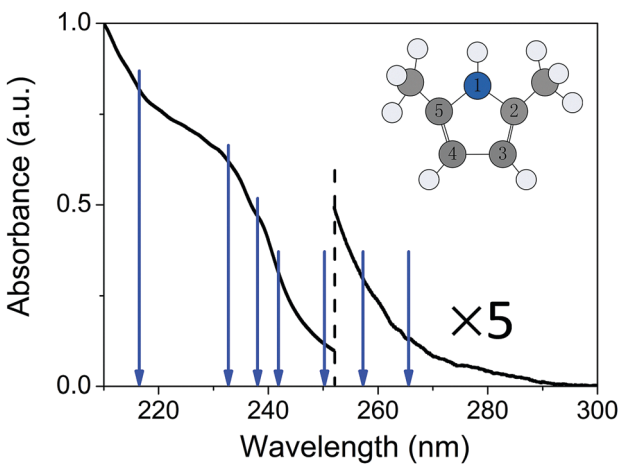

Fig. 1 The UV absorption spectrum of 2,5-DMP. The blue arrows indicate the pump wavelengths used in the current experiment.

[a] *State Key Laboratory of Molecular Reaction Dynamics, Dalian Institute of Chemical Physics, 457 Zhongshan Road, Dalian 116023, Liaoning, China. E-mail: wugr@dicp.ac.cn*
[b] *University of Chinese Academy of Sciences, Beijing 100049, China*

by transitions to the $^1\pi$3p Rydberg states, most of which gain intensities by vibronic coupling with the higher-lying $^1\pi\pi^*$ states. The strongly electric dipole allowed transitions to the $^1\pi\pi^*$ states should only become dominant at even shorter wavelengths. From 250 nm to longer wavelengths, there is a weak, broad band which should be due to the transitions to the $^1\pi\sigma^*$ states. It should be noted that in a resonance-enhanced multiphoton ionization (REMPI) spectra study of 2,5-DMP,[15] a broad and structured (1 + 1) REMPI spectrum over the wavelength range of 277.8–235.3 nm was attributed to the transition to the $B_2(^1\pi\pi^*)$ state which contradicts the present consensus on the understanding of the UV absorption spectrum of pyrrole. In the current study, the analysis of the experimental data is based on the assignments of Neville and Worth and a consistent picture is achieved.

The photodissociation dynamics of 2,5-DMP was investigated following excitations at 193.3 nm and at many near UV wavelengths in the range of 244–282 nm by Ashfold and coworkers by combining the H Rydberg atom photofragment translational spectroscopy, UV absorption spectrum and (1 + 1) REMPI spectrum techniques.[12] The deduced fragmentation dynamics show parallels with those of the bare pyrrole. It was concluded that the excitation at longer wavelengths leads to the (vibronically induced) population of the $S_1(^1\pi\sigma^*)$ state, and once the wavelength decreases to $\sim$250 nm, stronger, dipole allowed transitions to the excited states lying above the $S_1(^1\pi\sigma^*)$ state become apparent. Ovejas *et al.* investigated the relaxation dynamics of 2,5-DMP after excitations in the 290–239 nm range by time-resolved ion and photoelectron techniques.[16] It was suggested that excitation at the wavelength range of 286–255 nm results into the excitation of the $S_1(^1\pi\sigma^*)$ state and an invariant lifetime of $\sim$55 fs was derived. The excitation at shorter pump wavelengths was attributed to the transition to the $B_2(^1\pi\pi^*)$ state having a lifetime of $\sim$100 fs. Direct transfer to the ground state was proposed as the main decay channel of the $B_2(^1\pi\pi^*)$ state.

In this paper, we present a time-resolved photoelectron imaging (TRPEI) study of the ultrafast excited-state dynamics of 2,5-DMP over the wavelength range of 265.7–216.7 nm. It is found that excitation at longer wavelengths (265.7, 257.1 and 250.2 nm) results in excitation of the $S_1(^1\pi\sigma^*)$ state, for which a time constant of $\sim$90 fs is derived. At shorter pump wavelengths (242.1, 238.1, 232.6, and 216.7 nm), the excitations are tentatively assigned to the transitions to the $^1\pi$3p Rydberg state(s), which has a lifetime of 159 $\pm$ 20 fs at 242.1 nm, decreasing with the decrease of the pump wavelength, up to 88 $\pm$ 10 fs at 216.7 nm. In Section II, we describe the experimental method used. In Section III, the analysis of the experimental data and detailed discussion of the excited-state dynamics of 2,5-DMP are given. In Section IV, short conclusions are provided.

II Experimental

The experiment was carried out in a same way as that described in ref. 11, on a velocity map imaging (VMI) spectrometer.[17] Seven different pump wavelengths in the range of 265.7–216.7 nm were employed and the probe laser beam was fixed at 292.0 nm (1.0–1.3 μJ per pulse). All pump and probe laser beams were obtained from a fully integrated femtosecond Ti:Sapphire oscillator-regenerative amplifier (Coherent, Libra-HE, $<$50 fs, 800 nm, 3.8 mJ and 1 kHz). Two commercial optical parametric amplifiers with their respective UV wavelength extension package (OPA, Coherent, OPerA-Solo) were used, each pumped by a fraction (1.3 mJ per pulse) of the fundamental output of the amplifier. The probe laser pulse was directly obtained from one of the OPAs and all pump wavelengths were generated with the second OPA in two different ways, depending on the wavelength. Those in the range of 265.7–238.1 nm (0.4–0.8 μJ per pulse) were directly obtained from the second OPA. For pump laser pulses at 232.6 and 216.7 nm (0.2–0.4 μJ per pulse), the output of this OPA at 555.8 and 472.9 nm ($>$20 μJ per pulse) was mixed with a 400 nm laser beam ($\sim$50 μJ per pulse) using an β-BBO crystal (0.15 mm) respectively, which itself was the doubling of a fraction ($\sim$300 μJ per pulse) of the amplifier fundamental output using another β-BBO crystal (0.1 mm). The pump and probe laser pulses were combined collinearly on a dichroic mirror without further compression, and then focused using an f/75 lens into the interaction region of the VMI spectrometer to intersect a seeded 2,5-DMP molecular beam. A computer-controlled linear translation stage (Newport, M-ILS250HA) located upstream of the first OPA enabled precise control of the temporal delay between the pump and probe laser pulses. The pump–probe time delays were scanned back and forth multiple times to minimize any small hysteresis effects, and the effects caused by the fluctuations and drifts in the laser pulse energies, pointing, molecular beam intensity, *etc.*

The 2,5-DMP sample was obtained commercially (Adamas, $\geq$99%) and used without any further purification. The seeded molecular beam was generated by bubbling He of $\sim$4.0 bars through the liquid 2,5-DMP sample at room temperature using an Even-Lavie pulsed valve operated at 1 kHz and entered into the interaction chamber of the VMI spectrometer through a 1 mm skimmer (Beam Dynamics, Model 1). The pump pulse excited the 2,5-DMP molecules from their ground state to one or more electronically excited states by one-photon absorption, whereupon the delayed probe pulse produced photoelectrons *via* one-photon ionization. Care was taken to assure that the photoelectron signal from 2,5-DMP clusters was negligible. Both the pump and probe pulses were linearly polarized and the polarization direction was parallel to that of the micro channel plate (MCP) detector. Photoelectron images arising from the pump or the probe laser alone were also recorded. The sum of the single-color photoelectron images was subtracted in order to correct for background photoelectrons generated from single-color multiphoton ionizations. The 2D photoelectron images were transferred to the 3D distributions using the polar basis function expansion method.[18] The time-dependent photoelectron 3D distributions were further integrated along the recoiling angle to derive the photoelectron kinetic energy distributions, *i.e.*, time-resolved photoelectron spectra (TRPES). Electron kinetic energy calibration was performed

using multiphoton ionization of the Xe atoms. The cross-correlation (*i.e.*, instrumental response function (IRF)) between the pump and probe laser pulses was measured by the two-color 1 + 1′ non-resonant ionization of nitric oxide, except for the two longest wavelengths, 257.1 and 265.7 nm. At these two longest pump wavelengths, the 1 + 1′ pump–probe photon energy is below the ionization potential of the NO molecule and no measurement of the IRFs was performed. The delay-dependent curves of the electron yield were fitted, based on the approximation that both the pump and probe laser pulses have a Gaussian profile. The derived IRFs are 170 ± 2, 175 ± 4, 172 ± 3, 135 ± 4 and 134 ± 3 fs for the pump wavelengths of 250.2, 242.1, 238.1, 232.6 and 216.7 nm, respectively. The error bars represent one standard deviation. This process also served to determine the time-zero which was checked before and after the TRPEI measurements to make sure that there was no significant time-zero shift during the measurements.

In addition, the UV absorption spectrum of 2,5-DMP was measured under saturated vapor conditions at room temperature using a commercial UV-visible spectrometer (Jasco, V-650), as shown in Fig. 1.

III Results and discussion

At longer pump wavelengths

The TRPES spectra of 2,5-DMP at pump wavelengths of 265.7, 257.1 and 250.2 nm are shown in Fig. 2(a–c). The energetic limits for ionization to the ground (D_0) and first excited state (D_1) of 2,5-DMP cation, calculated using the previously reported respective ionization potentials of 7.58 and 8.73 eV,[19] are indicated by two white, vertical dash lines, respectively. At all these pump wavelengths, the photoelectron spectra are very similar to each other, with a strong, broad and a weak, narrow structure at the D_0 and D_1 energetic limits, respectively. The delay dependence of the photoelectron signal shows an extremely fast decay, with no clearly observable dynamics. In Fig. 2(d–f), the photoelectron kinetic energy distributions are shown, derived by integrating the TRPES spectra over a delay range of −100 to 100 fs within which the TRPES spectra have appreciable signals. It is clear that the whole photoelectron kinetic energy distributions, especially the features close to the D_0 and D_1 energetic limits shift to higher kinetic energies with the increase of the pump photon energy except the feature at

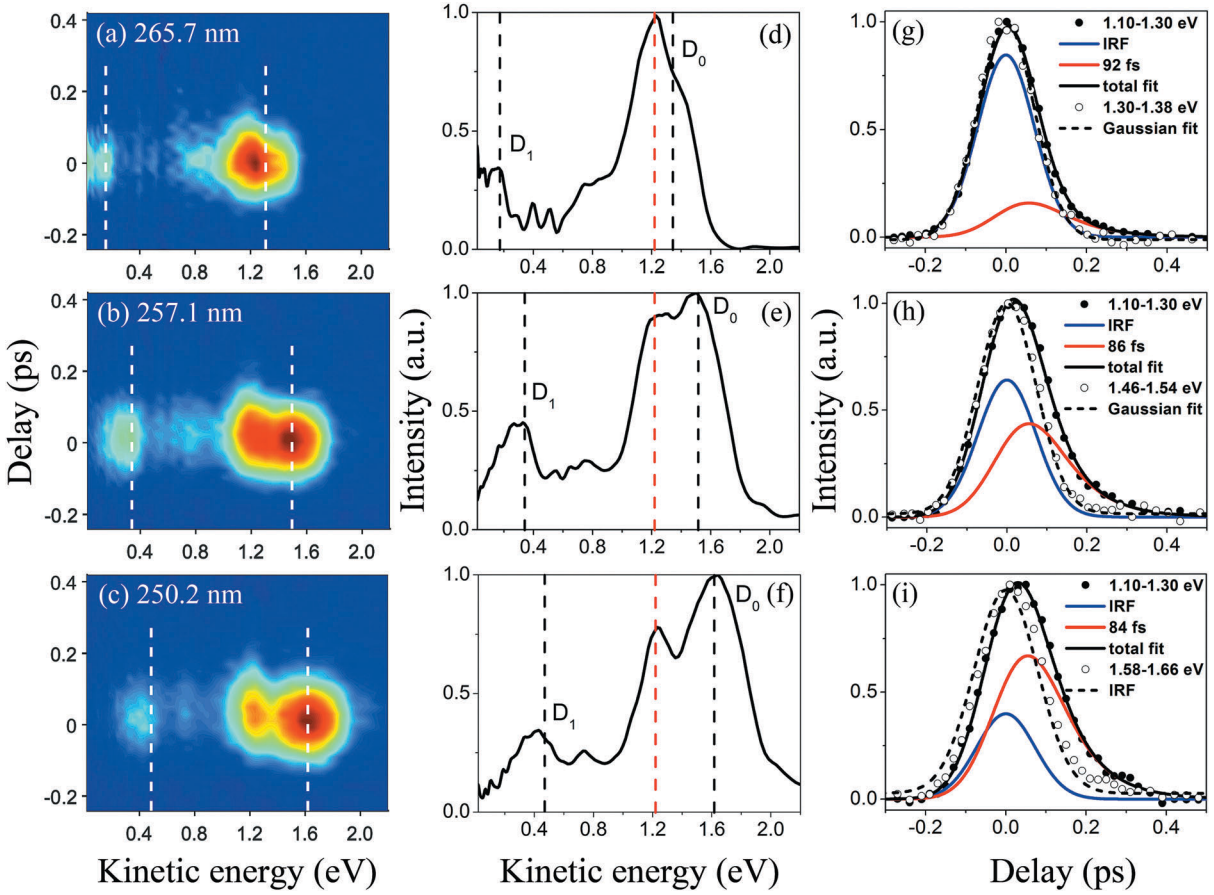

Fig. 2 (a–c) TRPES spectra of 2,5-DMP at pump wavelengths of 265.7, 257.1 and 250.2 nm, respectively. The background photoelectrons generated from single-color multiphoton ionization have been subtracted. The energetic limits to the ground and first excited state of cation at each pump wavelength are indicated by the white dash lines, respectively. (d–f) The photoelectron kinetic energy distributions derived by integrating the TRPES spectra from the −100 fs to 100 fs pump–probe delays. (g–i) Normalized transients for photoelectrons around 1.22 eV and of kinetic energies close to the ionization limit of D_0. The symbols show the experimental data, while the lines show the fits to the experimental data.

1.22 eV which stays invariant. The amount of the shift is close to the change of the pump photo energy. These characters are exactly the same as those observed previously in the study of the excited-state dynamics of 2,4-DMP.[11] Therefore, the analysis of the TRPES spectra of 2,5-DMP at these longer pump wavelengths can be proceeded in an analogous manner and the photoelectrons at 1.22 eV and other kinetic energies are assigned to the $S_1(^1\pi\sigma^*)$ state and from the 1 + 1′ non-resonant photoionization process.

There are two more factors in support of the assignation of the features observed at these longer pump wavelengths: (1) integrating the TRPES spectra over a kinetic energy range, a kinetic energy specific photoelectron transient is derived. In Fig. 2(g–i), the photoelectron transients at 1.22 eV (1.10–1.30 eV) and higher kinetic energies where a strong peak in TRPES spectra is located are shown and compared with each other. The photoelectron transient at higher kinetic energies for 250.2 nm can be very well represented with the IRF at this pump wavelength, derived independently. As for 265.7 and 257.1 nm, there are no independently measured IRFs and the photoelectron transients at higher kinetic energies are fitted with a Gaussian function. The fit qualities are very good and a full width at half maximum (FWHM) of 164 ± 2 and 169 ± 2 fs is derived for 265.7 and 257.1 nm, respectively. These widths show consistency with the one at 250.2 nm (170 ± 2 fs), validating the assignment of the photoelectron at higher kinetic energies to the 1 + 1′ non-resonant ionization. The photoelectron transients at 1.22 eV are clearly delayed and broader than the corresponding one at higher kinetic energies, indicating a decay dynamics for the 1.22 eV feature. The photoelectron transients at 1.22 eV are fitted with a model consisting of an exponential decay function convoluted with the corresponding IRF (for pump wavelengths of 265.7 and 257.1 nm, the FWHM widths derived from the fits to the higher kinetic energy photoelectron transients were used) and the corresponding IRF itself to account for contributions from the $S_1(^1\pi\sigma^*)$ state and the 1 + 1′ non-resonant photoionization, respectively. The fit qualities are satisfactory and lifetimes of 92 ± 25, 86 ± 20 and 84 ± 10 fs are derived for the pump wavelengths of 265.7, 257.1 and 250.2 nm, respectively. (2) As explained in the previous paper of 2,4-DMP,[11] the kinetic energy (ε_k) of the photoelectron corresponding to the $S_1(^1\pi\sigma^*)$ state can be calculated with the following equation,

$$\varepsilon_k = h\nu_{pr} - (IP_a - AEE) \quad (1)$$

where $h\nu_{pr}$, IP_a and AEE represent the probe photon energy, the adiabatic ionization potential and the adiabatic excitation energy of the $S_1(^1\pi\sigma^*)$ state. The ε_k, $h\nu_{pr}$ and AEE are 1.22 eV, 4.25 eV (292.0 nm) and 4.34 eV,[12] respectively. A photoelectron kinetic energy of 1.22 eV gives an adiabatic ionization potential of 7.37, which seems to be very reasonable, as compared to the reported vertical ionization potential of 7.58 eV.[19]

These experimental results are generally consistent with those from the study by Ovejas *et al.* in which a lifetime of ~55 fs was derived and was invariant within the pump wavelength range of 286–255 nm. However, the time constants derived in the current study are clearly longer. This might be simply due to a deeper ionization window (the evolution region of the wavepacket on the potential energy surface in which the probe photon can ionize the molecule) since a shorter probe wavelength was used.

At shorter pump wavelengths

The TRPES spectra of 2,5-DMP at the pump wavelengths of 242.1, 238.1, 232.6 and 216.7 nm are shown in Fig. 3(a–d). At all these four pump wavelengths, the photoelectron spectra are dominated by a strong, narrow peak around 1.9 eV. The contribution from photoelectrons at lower kinetic energies (below 1.6 eV) varies with the change of the pump wavelength. At 216.7 nm, a very weak feature (>2.2 eV) beyond the dominant peak at 1.9 eV starts to emerge. The delay dependence of the photoelectron signals show clear dynamics. In order to extract more detailed information from these TRPES data, a 2D global least-squares method was employed to simultaneously fit data at all time delays and photoelectron kinetic energies. It was found that a model giving a satisfactory fit consists of three components: a single exponential decay function convoluted

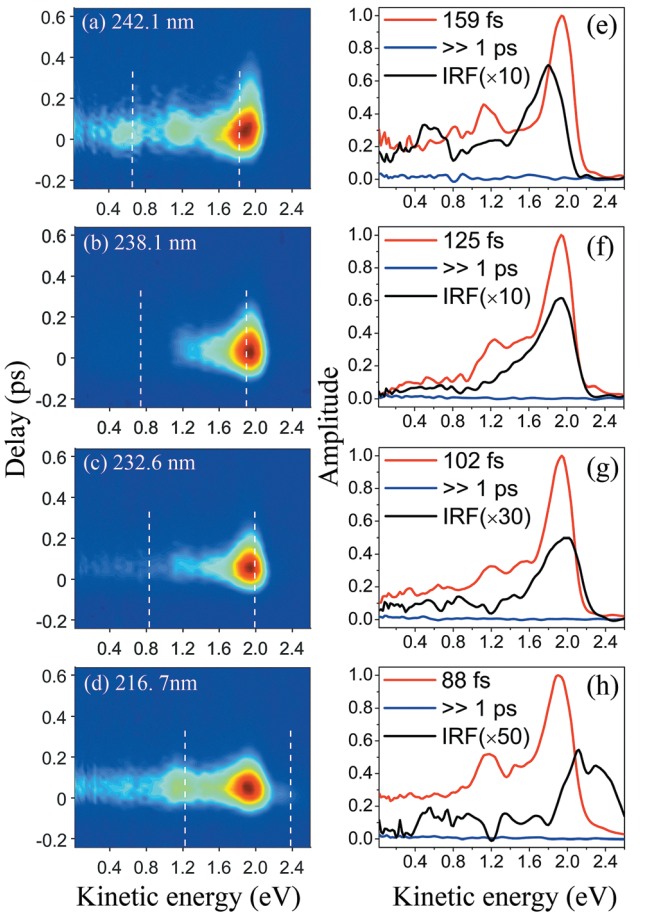

Fig. 3 (a–d) TRPES spectra of 2,5-DMP at pump wavelengths of 242.1, 238.1, 232.6 and 216.7 nm, respectively. The background photoelectrons generated from single color multiphoton ionization have been subtracted. (e–h) The photoelectron kinetic energy dependent amplitudes of each component derived from a 2D global least-squares fit to the data.

with the corresponding IRF, a very long lived component and the corresponding IRF. The derived photoelectron kinetic energy dependent amplitudes for these three components are shown in Fig. 3(e–h). The derived time constants for the exponentially decaying component are 159 ± 20, 125 ± 15, 102 ± 10 and 88 ± 10 fs at the pump wavelengths of 242.1, 238.1, 232.6 and 216.7 nm, respectively. In the data analysis, time-zeros were varied in the range of the time-zero drifts experimentally measured and the cross-correlations were also varied in the range of their uncertainties to obtain a best fit (minimum χ^2). This analysis also served to estimate the confidence intervals of the time constants.

The component ($\gg$1 ps) which shows no decay within the experimental scanning range (1 ps) has a very small amplitude over the whole range of photoelectron kinetic energy. This contribution could be from the photoionization of the metastable intermediate products or the final products from the photochemical processes of 2,5-DMP after one photon excitation. As for the component represented by the corresponding IRF, it is associated with a zero time constant. The amplitude is also very small and decreases rapidly with the increase of the pump photon energy. This might be due to a small contribution from the two-color non-resonant ionization. These two components are out of the scope of the current study and no further discussion will be provided.

The single exponentially decaying component corresponds to the electronic state(s) excited by the pump photon and the photoelectron kinetic energy dependent amplitudes derived from the fit correspond to the partial photoionization cross sections of the electronically excited state(s). From Fig. 3(e–h), it is evident that the partial photoionization cross sections are basically invariant with the change of the pump wavelength: the peaks at 1.2 and 1.9 eV stay invariant although there is 0.6 eV difference in the photon energies between 242.1 and 216.7 nm. The TRPES spectra at these shorter pump wavelengths show clear differences with those at longer pump wavelengths, suggesting that different electronic state(s) other than the $S_1(^1\pi\sigma^*)$ state should be involved. This is also consistent with the UV absorption spectrum in which a fast rise appears around 250 nm, indicating the onset of much stronger transition(s) to another electronic state(s). There is no solid assignment of the UV absorption spectrum of 2,5-DMP available. By an analogous assignment of the UV absorption spectrum of pyrrole, the broad, strong absorption band in the wavelength range of 250–210 nm, especially the long wavelength part of this band, should be dominated by transitions to the states of Rydberg character, mainly the $^1\pi$3p Rydberg states and the $S_2(^1\pi\sigma^*)$ state.[14] These states are highly mixed in their electronic characters and strong intensity borrowing effects are present. At the short wavelength end of this band, the electric dipole allowed transitions to the $^1\pi\pi^*$ states start to contribute and become dominating at an even shorter wavelength.[13] The invariant dominant peak at 1.9 eV is also reminiscent of a Rydberg state for which the ionization step is dominated by the $\Delta\nu$ = 0 diagonal transitions and a sharp peak in the photoelectron spectrum is usually derived. Therefore, it is very unlikely that the $^1\pi\pi^*$ states are responsible for the main features observed at these pump wavelengths and the components observed should be associated with the lower-lying Rydberg states. As for the $S_2(^1\pi\sigma^*)$ state, it is not expected that it dominates the absorption spectrum over such a wide wavelength range. Therefore, we tentatively assign the components observed at these shorter pump wavelengths to the $^1\pi$3p Rydberg state(s). Further theoretical calculations, including the simulation of the UV absorption spectrum, wave packet propagation, and photoionization cross section calculations, are needed to unambiguously identify the electronic states involved.

No clear clue of the decay channels of the $^1\pi$3p Rydberg state(s) was observed in the current TRPES spectra. The weak peak around 1.2 eV might suggest the presence of the $S_1(^1\pi\sigma^*)$ state, populated *via* internal conversion (IC) from the $^1\pi$3p Rydberg state(s). However, there is no clear delay of the photoelectron transient at 1.2 eV relative to that for the 1.9 eV dominant peak, in contradiction to what would be expected from the $^1\pi3p \rightarrow S_1$ IC process, suggesting that this 1.2 eV peak might not be due to the $S_1(^1\pi\sigma^*)$ state or the $S_1(^1\pi\sigma^*)$ state derived following the IC of the $^1\pi$3p Rydberg state(s) has a much shorter lifetime, caused by a much increased vibrational energy. Nevertheless, these TRPES spectra show that the IC from the $^1\pi$3p Rydberg state(s) to the $S_1(^1\pi\sigma^*)$ state represents at most a minor decay channel. One of the possible decay channels is the IC to the ground state directly. This channel is not detectable in the current experiment since one probe photon is not enough to ionize the ground state of 2,5-DMP.

The measured lifetimes and the observed decay mechanism of 2,5-DMP at these shorter pump wavelengths are in good agreement with the previous work by Ovejas *et al.* although in the latter the excitation was assigned to the $B_2(^1\pi\pi^*)$ state. Both studies suggested that IC to the $S_1(^1\pi\sigma^*)$ state is at most a minor channel and the direct transfer to the ground state should be the main decay channel. A lifetime of ~100 fs was found at the wavelength range of 250–239 nm in their work, but in the current work a rapid decrease of the lifetime of this excited state, from 159 ± 20 fs at 242.1 nm to 88 ± 10 fs at 216.7 nm, was observed.

Methyl substitution effects on the excited-state dynamics of pyrrole

Comparison of the experimental results for 2,5-DMP with those for the bare pyrrole,[9,20–22] NMP[10] and 2,4-DMP[11] could provide some detailed insights into the methyl substitution effects on the excited-state dynamics of pyrrole. Here, we discuss two aspects: the decay lifetime of the $S_1(\pi\sigma^*)$ state and the decay mechanism of the $^1\pi$3p Rydberg state. For the bare pyrrole, lifetimes $\lesssim$50 fs have been reported at pump wavelengths of $<$250 nm.[9,20,21] At 250 nm, a more than twice longer lifetime (126 fs) was reported.[21] This was attributed to the small barrier along the N–H dissociation coordinate and the population in the Franck–Condon (FC) region has to escape *via* tunnelling. For the methyl-substituted derivatives with methyls on the pyrrole ring, 2,4-DMP and 2,5-DMP, lifetimes of $<$30 and ~90 fs were derived from our studies,[11] respectively. Stavros and coworkers have reported time constants around 120 fs for the N–H bond

dissociation along the repulsive $S_1(\pi\sigma^*)$ state surface of 2,4-DMP.[23] These studies also show that the lifetime of the $S_1(\pi\sigma^*)$ state stays invariant with the change of the pump wavelength for 2,4-DMP and 2,5-DMP. For NMP, a dramatic difference was observed: the lifetime of the $S_1(\pi\sigma^*)$ state is around one to three orders of magnitude larger than that for pyrrole.[24] As we have discussed in the previous paper on 2,4-DMP,[11] the difference in the methyl-substitution effects on the topology of the $S_1(\pi\sigma^*)$ state surface due to the different substitution positions (N atom *vs.* the pyrrole ring) could be invoked to qualitatively explain these methyl substitution effects on the lifetime of the $S_1(\pi\sigma^*)$ state. However, as also suggested in the work of Ovejas *et al.*,[16] the nature of the multi-dimensionality of the potential energy surfaces of pyrrole and its derivatives has to be taken in account in order to give a complete description of the decay dynamics of the $S_1(\pi\sigma^*)$ state and its methyl substitution effects. In this sense, a multi-dimensional dynamic simulation might be the most insightful.

The second aspect to be discussed here is the methyl substitution effects on the decay mechanism of the $^1\pi3p$ Rydberg state. In our previous paper on NMP,[10] the excited state at 217 nm was assigned to the $B_1(^1\pi3p_y)$ state and IC to the $S_1(\pi\sigma^*)$ state was clearly observed and represents a main decay channel of the $B_1(^1\pi3p_y)$ state. For 2,4-DMP, the IC to the $S_1(\pi\sigma^*)$ state was also observed, but only represents a minor decay channel of the $^1\pi3p$ Rydberg state(s) over the pump wavelength range of 231.8–199.7 nm. For 2,5-DMP, no clear clue of the involvement of the $S_1(\pi\sigma^*)$ state was observed in the decay of the $^1\pi3p$ Rydberg state(s) over the excitation range of 242.1–216.7 nm, suggesting IC to the $S_1(\pi\sigma^*)$ state is at most a minor channel. The most like decay channel for the $^1\pi3p$ Rydberg state of the latter two derivatives is IC directly to the ground state, presumably enabled by the ring puckering vibrational modes. These observations suggest a difference in the methyl substitution effects on the decay mechanism of the $^1\pi3p$ Rydberg state. Methyl substitution on the pyrrole ring seems to enhance the channel of direct IC to the ground state, either by enhancing the ring puckering channel or through the additional vibronic coupling between the $^1\pi3p$ Rydberg state and the ground state involving the additional vibrational modes from the methyl groups. As for the methyl substitution on the N atom, these effects seem less important and the IC to the $S_1(\pi\sigma^*)$ state represents a main channel.

IV Conclusions

The dynamics of 2,5-DMP following excitation at wavelengths in the range of 265.7–216.7 nm are studied with the TRPEI technique. We conclude that excitation at longer wavelengths (265.7, 257.1 and 250.2 nm) results in population of the $S_1(^1\pi\sigma^*)$ state, consistent with previous studies. The $S_1(^1\pi\sigma^*)$ state decays out of the photoionization window with a lifetime of $\sim$90 fs, invariant with the pump wavelength. At shorter pump wavelengths (242.1, 238.1, 232.6 and 216.7 nm), the assignments are less clear-cut. We tentatively assign the transitions to the $^1\pi3p$ Rydberg state(s), having lifetimes of 159 ± 20, 125 ± 15, 102 ± 10 and 88 ± 10 fs at 242.1, 238.1, 232.6 and 216.7 nm, respectively. No clear clue of IC to the $S_1(^1\pi\sigma^*)$ state was observed, indicating it represents at most a minor decay channel of the $^1\pi3p$ Rydberg state(s). Methyl substitution effects on the excited-state dynamics of pyrrole are discussed by comparing the experimental results for the bare pyrrole, NMP, 2,4-DMP and 2,5-DMP. Methyl substitution on the pyrrole ring seems to enhance the channel of direct IC from the $^1\pi3p$ Rydberg state to the ground state, either by enhancing the ring puckering channel or through the additional vibronic coupling between the $^1\pi3p$ Rydberg state and the ground state involving the additional vibrational modes from the methyl groups. As for the methyl substitution on the N atom, these effects seem less important and the IC to the $S_1(\pi\sigma^*)$ state represents a main channel.

Conflicts of interest

There are no conflicts to declare.

Acknowledgements

This work was supported by the National Natural Science Foundation of China (21573228) and the Strategic Priority Research Program of the Chinese Academy of Sciences (No. XDB17000000).

References

1 S. White, J. W. Szewczyk, J. M. Turner, E. E. Baird and P. B. Dervan, *Nature*, 1998, **391**, 468.
2 E. Pazos, J. Mosquera, M. E. Vázquez and J. L. Mascareñas, *ChemBioChem*, 2011, **12**, 1958.
3 A. L. Sobolewski and W. Domcke, *Chem. Phys.*, 2000, **259**, 181.
4 A. L. Sobolewski, W. Domcke, C. Dedonder-Lardeux and C. Jouvet, *Phys. Chem. Chem. Phys.*, 2002, **4**, 1093.
5 M. N. R. Ashfold, B. Cronin, A. L. Devine, R. N. Dixon and M. G. D. Nix, *Science*, 2006, **312**, 1637.
6 M. N. R. Ashfold, G. A. King, D. Murdock, M. G. D. Nix, T. A. A. Oliver and A. G. Sage, *Phys. Chem. Chem. Phys.*, 2010, **12**, 1218.
7 G. M. Roberts, D. J. Hadden, L. T. Bergendahl, A. M. Wenge, S. J. Harris, T. N. V. Karsili, M. N. R. Ashfold, M. J. Paterson and V. G. Stavros, *Chem. Sci.*, 2013, **4**, 993.
8 G. M. Roberts and V. G. Stavros, *Chem. Sci.*, 2014, **5**, 1698.
9 G. R. Wu, S. P. Neville, O. Schalk, T. Sekikawa, M. N. R. Ashfold, G. A. Worth and A. Stolow, *J. Chem. Phys.*, 2015, **142**, 074302.
10 G. R. Wu, S. P. Neville, O. Schalk, T. Sekikawa, M. N. R. Ashfold, G. A. Worth and A. Stolow, *J. Chem. Phys.*, 2016, **144**, 014309.
11 D. Y. Yang, Z. C. Chen, Z. G. He, H. D. Wang, Y. J. Min, K. J. Yuan, D. X. Dai, G. R. Wu and X. M. Yang, *Phys. Chem. Chem. Phys.*, 2017, **19**, 29146.
12 B. Cronin, M. G. D. Nix, A. L. Devine, R. N. Dixon and M. N. R. Ashfold, *Phys. Chem. Chem. Phys.*, 2006, **8**, 599.

13 T. Geng, O. Schalk, S. P. Neville, T. Hansson and R. D. Thomas, *J. Chem. Phys.*, 2017, **146**, 144307.
14 S. P. Neville and G. A. Worth, *J. Chem. Phys.*, 2014, **140**, 034317.
15 J. M. Beames, M. G. D. Nix and A. J. Hudson, *J. Chem. Phys.*, 2009, **131**, 174305.
16 V. Ovejas, R. Montero, M. Fernández-Fernández and A. Longarte, *J. Phys. Chem. A*, 2015, **119**, 3355.
17 Z. G. He, Z. C. Chen, D. Y. Yan, D. X. Dai, G. R. Wu and X. M. Yang, *Chin. J. Chem. Phys.*, 2017, **30**, 247.
18 G. A. Garcia, L. Nahon and I. Powis, *Rev. Sci. Instrum.*, 2004, **75**, 4989.
19 B. Kovac, L. Klasinc, J. Vorkapic-Furac, M. Mintas and J. V. Knop, *J. Chem. Soc., Perkin Trans. 2*, 1997, 2597.
20 R. Montero, A. Peralta Conde, V. Ovejas, M. Fernandez-Fernandez, F. Castano, J. R. Vazquez de Aldana and A. Longarte, *J. Chem. Phys.*, 2012, **137**, 064317.
21 G. M. Roberts, C. A. Williams, H. Yu, A. S. Chatterley, J. D. Young, S. Ullrich and V. G. Stavros, *Faraday Discuss.*, 2013, **163**, 95.
22 O. M. Kirkby, M. A. Parkes, S. P. Neville, G. A. Worth and H. H. Fielding, *Chem. Phys. Lett.*, 2017, **683**, 179.
23 M. Staniforth, J. D. Young, D. R. Cole, T. N. V. Karsili, M. N. R. Ashfold and V. G. Stavros, *J. Phys. Chem. A*, 2014, **118**, 10909.
24 L. Blancafort, V. Ovejas, R. Montero, M. Fernández-Fernández and A. Longarte, *J. Phys. Chem. Lett.*, 2016, **7**, 1231.